GAMMA-RAY IMAGING WITH A ROTATING HEXAGONAL UNIFORMLY REDUNDANT ARRAY

W. R. Cook, M. Finger, T. A. Prince, and E. C. Stone
California Institute of Technology, Pasadena, CA 91125

Abstact

Laboratory experiments have been performed to demonstrate the capabilities of a γ-ray imaging system employing a NaI Anger camera and a rotating coded aperture mask. The mask incorporates in its design a new type of hexagonal uniformly redundant array (HURA) which is essentially antisymmetric under 60° rotation. The image formation techniques are described and results are presented that demonstrate the imaging capability of the system for individual and multiple point sources of γ-ray emission. The results are compared to analytical predictions for the imaging and point source localization capabilities of coded aperture systems using continuous detectors.

Introduction

Coded aperture imaging is a well known technique for producing images of x-ray and γ-ray photon sources. The basic technique involves the use of an aperture consisting of opaque and transparent elements to cast a shadow on a position sensitive detector. The image of the source region is reconstructed from the information contained in the detected photon spatial distribution.

Considerable attention has been given to finding suitable patterns for the coded aperture, yielding a variety of solutions including random hole masks[1] and uniformly redundant arrays[2,3]. The studies presented here have been motivated by the desire to apply coded aperture techniques to the imaging of astrophysical sources of hard x-rays and γ-rays (30 keV - 5 MeV). Several characteristics differentiate astrophysical γ-ray imaging in this energy range from imaging at lower photon energies. In particular, the weak flux of γ-rays from astrophysical sources combined with large, variable γ-ray backgrounds requires that coded aperture techniques be optimized for operation at low signal to noise ratio and for reduction of systematic errors in the image formation process.

A key feature in the approach described in this paper is the introduction of time modulation into the image coding process through the rotation of recently developed hexagonal celled uniformly redundant arrays (referred to hereafter as HURAs). The HURAs, two of which are shown in Figure 1, are based on Hadamard cyclic difference sets and are constructed as described in detail in Cook et. al. 1983[4]. The HURAs offer the following advantages for γ-ray imaging:

1) The HURAs are nearly half open and half closed. This yields optimum flux sensitivity for the detection of weak γ-ray sources. At any instance a given source is viewed by half of the detector (or detector array) which measures the source plus background flux while the other half measures the background flux only. The simultaneous measurement of source plus background and background in different parts of the detector reduces sensitivity to time variations of the detector background counting rate. This tolerance of time variations of the detector background rate is particularly important in astrophysical γ-ray observations where time variations of the background are almost unavoidable due to motion of the detector in either the high altitude balloon or space environments.

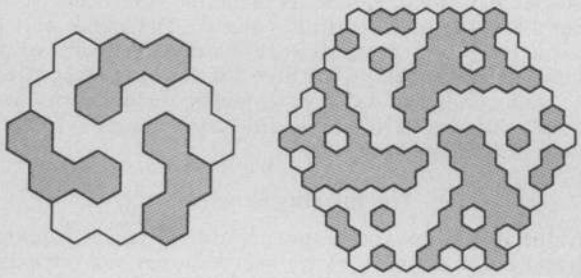

Figure 1. HURA patterns with 19 and 127 elements.

2) The HURAs are antisymmetric upon 60 degree rotation. When the mask patterns are rotated 60 degrees the open and closed cells interchange position, except the cell in the center of the pattern which remains unchanged. This antisymmetry provides for cancellation of any spurious imaging effects due to spatial variations in the detector background counting rate. With the HURAs such background effects can be essentially removed by subtracting the count rate distributions obtained with the coded aperture in two positions, 60° apart.

3) An entire class of HURA patterns is available and is complete. That is, an HURA pattern with the desired properties of being half open/half closed and antisymmetric upon 60 degree rotation may be generated with a number of elements v if v is a prime number and if and only if there exist integer values i, j, and n such that $v = i^2+ij+j^2$ and $v = 4n-1$. The allowed values of v are rather closely spaced (the first few are v=3, 7, 19, 31, 43, 67, 79, 103, 127, 139, 163, 199 ...) such that the number of elements in the coded-aperture pattern may be appropriately matched to the number of spatial resolution elements in a given detector or detector array.

4) These nearly circular HURAs may be continuously rotated to allow extension of the field of view by repetition of the basic HURA pattern. The rotational motion eliminates the ambiguity that would normally result with a stationary mask having multiple repetitions of a basic pattern. This enlargement of the field of view and corresponding increase in the number of pixels in the image can be accomplished with no increase in the size or resolution of the detector.

The technique of time modulation with rotating antisymmetric HURA's is very effective in eliminating potential systematic errors due to spatial and temporal background nonuniformities. In this paper, we will describe the technique of imaging with rotating HURA's, present results of laboratory demonstrations of an imaging system using this concept, and discuss the general capabilities of the approach.

0018-9499/84/0002-0771$01.00 © 1984 IEEE

Experimental Setup

Our apparatus consisted of a standard NaI Anger camera plate and an HURA coded aperture consisting of multiple repetitions of the basic 127 element HURA pattern shown in Figure 1. The total number of elements in the mask was approximately 1500. The NaI plate was 1.3 cm thick and was viewed by 19 two inch diameter photomultiplier tubes which were simultaneously pulse height analyzed. A position resolution of 1.7 mm rms was obtained at the 122 keV line of Co^{57}. The aperture was constructed of 1.2 mm thick lead cells bonded to a 0.5 mm thick aluminum plate which could be rotated continuously at 0.1 rpm. The mask cell spacing was chosen as 1.0 cm, such that the outside diameter of the 127 element basic HURA pattern was somewhat smaller than the 15 cm usable diameter of the camera plate. The mask and the Co^{57} source to be imaged were placed in front of the detector at distances of 0.3 and 3.0 meters, respectively. Both pulse height data and mask orientation were encoded on magnetic tape for subsequent computer analysis and image formation.

The Imaging Process

In our initial imaging experiments the mask remained stationary. The sources were observed over two periods of equal duration, and between these observations the mask was rotated by 60°, to its "antimask" state. During later experiments the mask was rotated continuously. Since the image formation process for continuous rotation involves the construction of many simpler "mask-antimask" images, we will first describe their construction. Along with this description we will present an analysis of the image and examples from an experiment with a single source and low background. We will then proceed to the case of the continuously rotating mask and finally discuss the detection of weak sources in the presence of large nonuniform detector background.

For the mask-antimask experiment a hexagonal region of the detector was chosen with the same area and orientation as the basic pattern of the mask, and events from within this region where binned by position. The distribution formed during the second ("antimask") observation period was then subtracted from that formed during the first, in order to eliminate the background level on a position by position basis. Let $\Delta Det(\vec{u})$ be this difference distribution as a function position $\vec{u}$ on the detector. The gray scale image in Figure 2 shows $\Delta Det(\vec{u})$ for our single source example. It is basically a blurred and shifted shadow of the mask pattern.

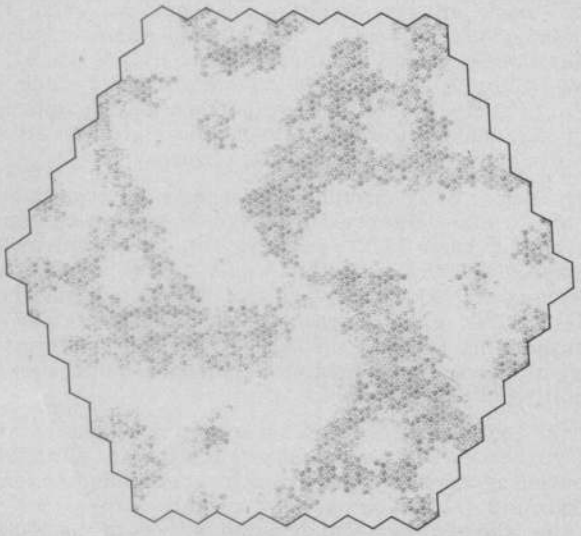

Figure 2. Gray scale representation of the difference shadow pattern ($\Delta Det(\vec{u})$, see text) due to a point source.

The initial source reconstruction map is created by a process called delta decoding[5]. For a bin located at $\vec{u}$ in the detected difference distribution $\Delta Det(\vec{u})$ and a mask cell centered at $\vec{v}_k$ the events are projected back to the source direction bin at $\vec{w}=\vec{v}_k-\vec{u}$ and added or subtracted depending on whether or not the mask cell is open or closed ($n_k = \pm 1$, $n_k = 0$ for the central mask cell). When this is done for all pairs of bins and mask cells the resulting map is on average flat except for peaks in the direction of sources. The source map is given by the expression:

$$SM(\vec{w}) = \sum_k n_k \Delta Det(\vec{v}_k - \vec{w}) \quad . \tag{1}$$

We desire that the source map be an optimal representation of the true source distribution. In fact, it can be shown that on the average:

$$\langle SM(\vec{w}) \rangle = \frac{\varepsilon \tau \upsilon}{2} \int Res(\vec{w} - \vec{w}_0) S(\vec{w}_0) d^2\vec{w}_0 \quad , \tag{2}$$

where:

ε is the detector efficiency;

τ is the total observation time;

υ is the number of cells in the basic HURA pattern;

$S(\vec{w}_0)$ is the source strength in direction $\vec{w}_0$;

$Res(\vec{w}-\vec{w}_0)$ is the angular response function for a point source

$\equiv h_{eff}(\vec{w}-\vec{w}_0) - \frac{1}{\upsilon}$;

$h_{eff}(\vec{w})$ is the detector response to a point source of γ-rays of unit flux viewed through a "pinhole" mask having a single hexagonal shaped hole. $h_{eff}(\vec{w})$ is formed by convolving a hexagon with the intrinsic position resolution of the detector.

Thus $\langle SM(\vec{w}) \rangle$ is simply the true source distribution convolved with the point source resolution function of the mask-detector system.

The source map (given by Equation 1) for our single source example is shown in Figure 3 in perspective. There is a single source peak with no other significant features. Figure 4 shows a comparison of the profile of the image peak with the expected average given by Equation 2 using the measured detector resolution and source strength. The prediction is in good agreement with the results.

Each bin in the source map represents data from a very limited area of the detector. The values of neighboring bins are independent, and so the image is noisy on short scales. To eliminate this high frequency noise and

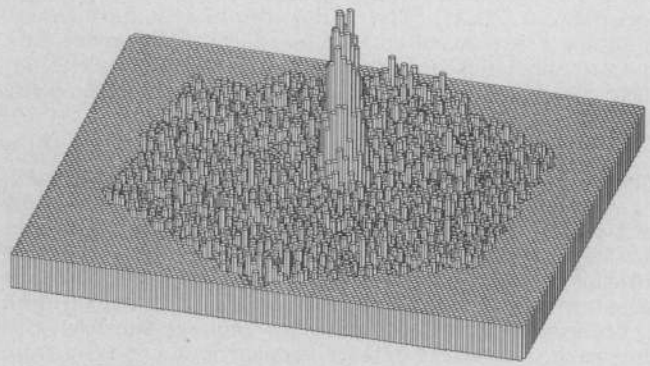

Figure 3. Source map reconstructed from the shadow pattern of Figure 2.

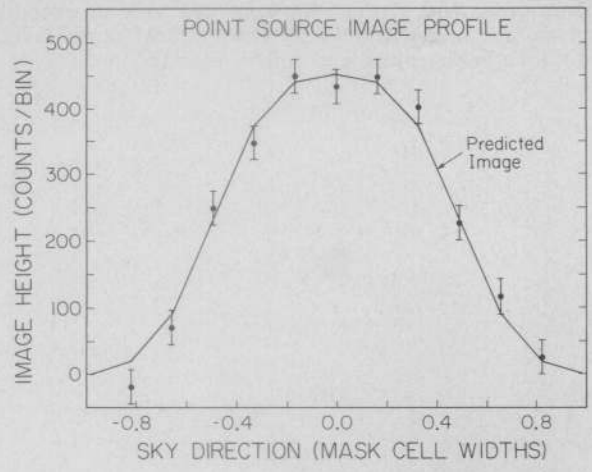

Figure 4. Comparison of the measured point source image profile and that predicted from the size of the mask cell and the detector position resolution.

obtain source strength and location measurements we next smooth the source map. The most significant flux measurement is obtained when the smoothing function is $h_{eff}(\vec{v})$. The resulting convolved source map is:

$$CSM(\vec{v}) = \int h_{eff}(\vec{v}-\vec{v}_0)SM(\vec{v}_0)d^2\vec{v}_0 \ . \qquad (3)$$

which is expected on average to be

$$<CSM(\vec{v})> = \frac{\varepsilon\tau A}{2}\int f(\vec{v}-\vec{v}_0)S(\vec{v}_0)d^2\vec{v}_0 \ . \qquad (4)$$

Here A is the detector area and the modified resolution function $f(\vec{v})$ is given by:

$$f(\vec{v}) = \frac{v}{A}\int h_{eff}(\vec{v}-\vec{v}_0)h_{eff}(\vec{v}_0)d^2\vec{v}_0 - \frac{1}{v} \ , \qquad (5)$$

which describes the form of a single source image. $f(\vec{v})$ is normalized such that the peak height $\bar{f} \equiv f(\vec{0})$ is $1-1/v$ for a detector of perfect resolution, and less than this value for a detector with finite resolution. For a single source experiment with a detector of perfect resolution the mask divides the detector into "source on" and "source off" regions. With finite position resolution the distinction between these regions is blurred, leading to a degradation of flux sensitivity. The peak height $\bar{f}$ is a measure of the degree of blurring. For our mask and detector $\bar{f} = .85$.

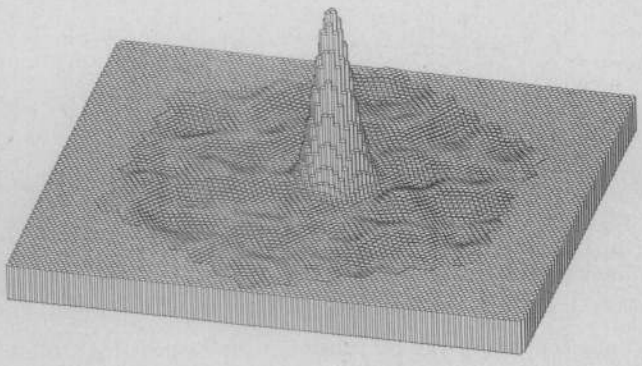

Figure 5. Convolved source map obtained by smoothing the image of Figure 3 with the point response function h_{eff} (see text).

Figure 5 shows the smoothed image for our single source example. The high frequency noise has been removed at the expense of increasing the width of the image peak. The remaining noise is seen as waves in the zero level. It can be shown that the average variance of the image from the expected mean (Equation 5) is uniform across the image and given by

$$\sigma^2_{CSM} = \bar{f}A\tau\left[B + \tfrac{1}{2}\varepsilon S\right] \ . \qquad (6)$$

where B is the average background rate and S is the total source flux. For a single source of strength S in the direction $\vec{v}_s$ the statistical significance of a flux measurement is given by:

$$\kappa \equiv \frac{<CSM(\vec{v}_s)>}{\sigma_{CSM}} = \frac{\varepsilon S}{2}\left[\frac{A\tau}{B+\frac{1}{2}\varepsilon S}\right]^{\frac{1}{2}} \times \bar{f}^{\frac{1}{2}} = \kappa_0 \bar{f}^{\frac{1}{2}} \ . \qquad (7)$$

Thus the significance is that of a "source on - source off" measurement, κ_0, multiplied by the factor $\bar{f}^{\frac{1}{2}}$. The larger the mask cell size, the closer $\bar{f}$ approaches 1, and the higher the sensitivity of the imaging system. However, this must be balanced against the angular resolution and angular localization capability of the system which are optimized for values of $\bar{f}$ smaller than 1.

The angular resolution or "pixel size" is directly related to the position resolution of the detector and the dimensions of a mask cell. For the case of interest where the rms detector position resolution is substantially smaller than the mask cell size (as required for good flux sensitivity) the pixel size is just given by:

$$\vartheta = \arctan\left(\frac{\Delta}{D}\right) \qquad (8)$$

where Δ is mask cell spacing and D is the mask to detector separation.

The angular source localization uncertainty can be shown to be:

$$\sigma_\vartheta = \arctan(\sigma_w / D) \ , \text{ where, } \sigma_w \equiv \frac{2}{\kappa_0}\left[\frac{1}{-\nabla^2 f(0)}\right]^{\frac{1}{2}} \ . \qquad (9)$$

The angular localization uncertainty is thus directly related to the curvature of the modified resolution function, $f(\vec{z})$, defined in Equation 5. Note that the angular localization uncertainty is inversely proportional to the significance of the source flux measurement. The mask cell size may be chosen to make the angular source location uncertainty σ_ϑ minimum. This minimum occurs for the cell width near 1.5 times the FWHM of the detector position resolution.

Continuous Mask Rotation

For simple mask-antimask imaging with a non-rotating periodic mask the image itself is periodic. Figure 6a shows one such image of a single source where now the image has been calculated over a much larger field than in Figure 5. The source location is ambiguous, the true source peak being repeated with the period of the mask. Continuous mask rotation removes this ambiguity allowing an extension of the field of view. With continuous mask rotation the data is first divided into sets corresponding to fixed mask orientation intervals, and these sets are then grouped into mask-antimask pairs. For each pair an image is formed as described above. The result is a series of images parameterized by mask rotation angle. The series of images contain the true source peak at a fixed location with the repeated peaks rotating about it. The result of adding the images together is shown in Figure 6b. The repeated peaks are blurred into a series of low rings centered on the peak at the true source location.

Since the location and amplitude of the rings are directly related to the location and amplitude of the peak, the rings may be subtracted, resulting in the final image in Figure 6c.

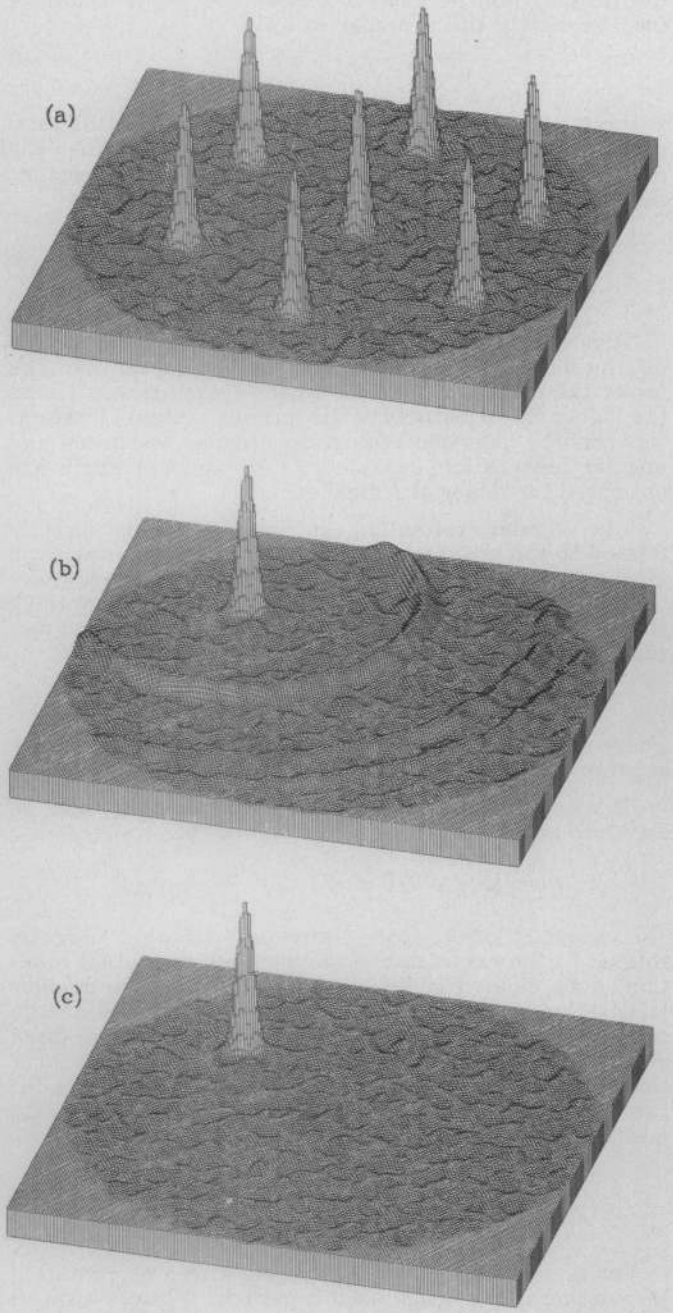

Figure 6. (a) Ambiguous image of a single point source obtained with an extend HURA which was not continuously rotated; (b) Image obtained with a continuously rotated HURA; (c) Image after ring removal.

Detection of Weak Sources

For astrophysical γ-ray observations it is important to understand the response of the imaging system to weak sources in the presence of nearby strong sources and in the presence of large nonuniform backgrounds.

The response of the system to a weak 6σ source ($\kappa = 6$) separated by two mask cell spacings from a strong source (60σ), is illustrated in Figure 7. The weak peak is clearly resolved from the strong, showing the lack of extended wings on the image function. The general noise level is due to both background and source events.

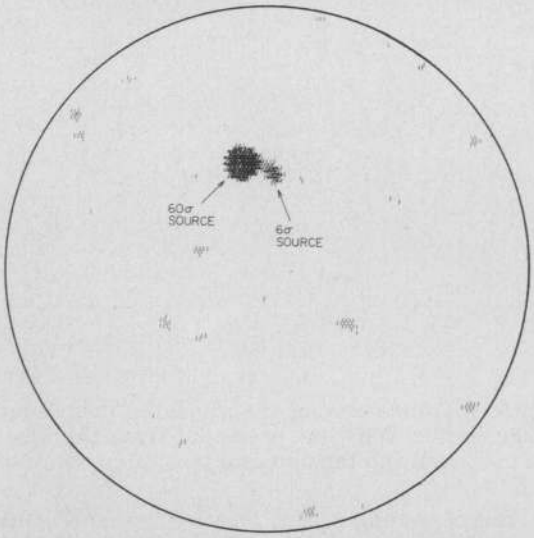

Figure 7. Gray scale image of a strong and a nearby weak source. The gray scale threshold is 2.5σ.

The response of the system to a weak source (6σ) in the presence of a large nonuniform background is illustrated in Figure 8. The nonuniform detector background was introduced with a second Co^{57} source placed near the detector, such that the background varied by a factor of two across the detector. The background to source flux ratio for the experiment was 100.

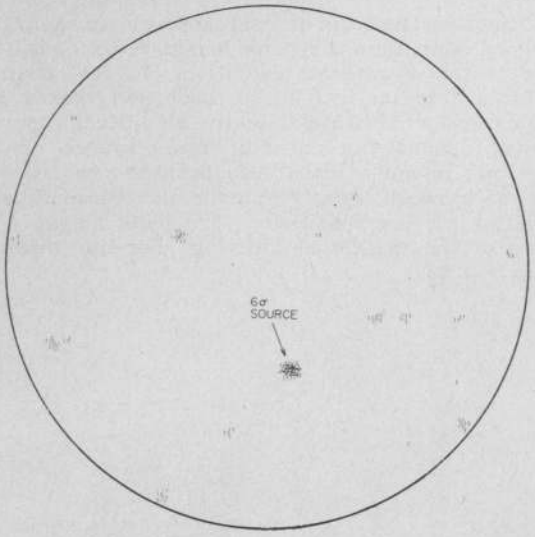

Figure 8. Gray scale image of a weak source taken in the presence of a large non-uniform detector background.

Note that while the 6σ source is the largest feature in the image, there are also several noise peaks above the 2.5σ gray scale threshold. How, in an astrophysical observation, are these noise peaks to be distinguished from a real source? Knowledge of the average image fluctuation level σ is not enough to answer this question, because σ tells us only the variation to be expected in the image at a

fixed point. If we search through the image for peaks we increase our chances of finding a large fluctuation. Thus to be confident in the identification of an unknown source we must know the expected distribution of noise peaks. Figure 9 shows a comparison of the distribution of noise peaks we predict with that actually found for the image in Figure 8. The agreement is good, and the 6σ peak (not included) is clearly not a part of the noise.

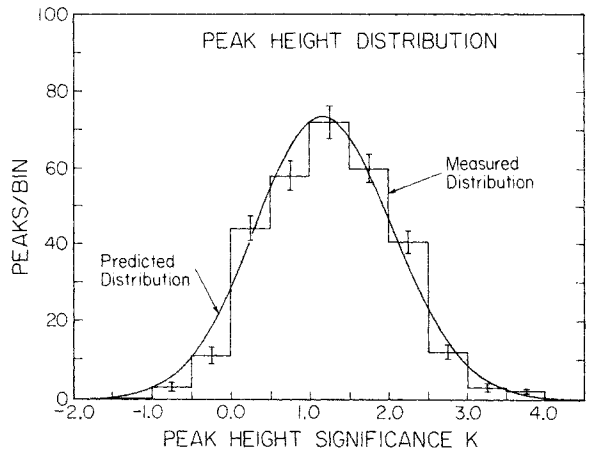

Figure 9. Comparison of the predicted and measured distribution of noise peak heights for the image of Figure 8.

Implications for Gamma-ray Astronomy

The technique of imaging with rotating HURAs described in this paper has been specifically designed to meet the needs of γ-ray astronomy. First generation instruments carried on high altitude balloons and based on currently available Anger camera plate technology will achieve flux sensitivity competitive with that of a standard "source on - source off" non-imaging experiment while imaging a rather wide (20°) field of view with 0.5 degree pixel size.

Specifically, NaI Anger cameras can be constructed with $\geq$1000 cm^2 area and position resolution of better than 0.5 cm rms over the energy range from 50 KeV to several MeV. If we match such a detector with an HURA coded aperture having a cell spacing of 2.2 cm we strike a good compromise between point source flux sensitivity and angular localization capability, achieving 74% of the flux sensitivity of a comparable non-imaging "source on - source off" experiment. A pixel size of 0.5 degrees is then obtained with a mask-detector separation of 2.5 meters. The point source localization uncertainty would be 5 arcminutes for a 5 sigma source.

Later generation instruments flown on board the Space Shuttle or exposed on a space platform will benefit from increased mask to detector separation and longer exposure time and could achieve 1 to 2 arcminute resolution with point source localization to a few arcseconds.

Acknowledgements

This work was supported in part by NASA grant NGR 05-002-160. We thank Prof. R. Vogt for numerous contributions to this work. We also acknowledge useful discussions on γ-ray imaging with colleagues at the Jet Propulsion Laboratory, the University of Chicago and the University of New Hampshire. In particular, we thank D. Forrest, J. Ling, R. Kroger, and Prof. D. Müller.

References

[1] R. H. Dicke, "Scatter-Hole Cameras for X-Rays and Gamma Rays," Ap. J. Lett., vol 153, pp. L101-L106, August 1968.

[2] J. Gunson and B. Polychronopulos, "Optimum Design of a Coded Aperture Mask X-Ray Telescope for Rocket Applications," Mon. Not. R. Astron. Soc., vol. 177, pp. 485-497, 1976.

[3] E. E. Fenimore and T. M. Cannon, "Coded aperture imaging with uniformly redundant arrays," Applied Optics, vol. 17, pp. 337-347, 1978.

[4] W. R. Cook, M. H. Finger and T. A. Prince, "Uniformly Redundant Arrays with Rotational Antisymmetry," in preparation.

[5] E. E. Fenimore, "Coded aperture imaging: the modulation transfer function for uniformly redundant arrays," Applied Optics, vol. 19, pp. 2465-2471, July 1980.